Imaging Lattice Defects and Distortions in Alkali-Metal Iodides Encapsulated within Double-Walled Carbon Nanotubes

Pedro M. F. J. Costa,*[,†,§] Steffi Friedrichs,[†,§] Jeremy Sloan,[†,‡] and Malcolm L. H. Green[†]

Inorganic Chemistry Laboratory, South Parks Road, Oxford, OX1 3QR, United Kingdom, and Department of Materials, Parks Road, Oxford, OX1 3PH, United Kingdom

Received February 9, 2005. Revised Manuscript Received April 4, 2005

The alkali-metal iodide double-walled carbon nanotube composites MI@DWNTs (M = K, Cs) have been prepared using a melt-phase filling procedure. The imaging and subsequent structural analysis of the encapsulated metal iodide crystals was performed with a combination of phase restored high-resolution transmission electron microscopy technique, structural modeling, and image simulation. The atomically resolved structures of the MI crystals were seen to contain several lattice defects including interstitials and vacancies as well as distortions of the crystal planes including shearing and rotation.

Introduction

Due to their hollow interior, single- (SWNTs) and multi-walled carbon nanotubes (MWNTs) can act as templates for one-dimensional crystal growth with the internal carbon walls constraining the diameter of the encapsulated material.[1−3] Successfully encapsulated substances include biomolecules and complex metal alloys.[4,5] Recently, attention has focused on double-walled carbon nanotubes (DWNTs), which, until the latest successes in selective synthesis of these structures, were often considered as a mere byproduct of SWNT and MWNT syntheses.[6,7] From a structural point of view, DWNTs are interesting because the wall spacing between the two graphene layers can be larger (up to 4.0 Å) than that usually observed in MWNTs (3.4−3.6 Å).[8,9] Applications of DWNTs have been proposed including their use in nanobearings or nanogears[10] and as high-quality field-emitters.[11] Moreover, the electronic versatility of DWNTs could give rise to arrangements such as SWNTs containing metallic inner nanotubes nested in outer semiconductor tubes.[12]

DWNTs, produced by chemical vapor deposition (CVD) methods, have been filled with fullerene molecules[13] and crystalline PbI_2.[14] Here, we report the synthesis of the composites MI@DWNT (where M = K, Cs) and their study using a transmission electron microscopy image restoration procedure in which the exit-surface wave function of the object is recovered from a focal series of images. This technique, which provides digital complex images of considerably improved resolution and additional restored phase-information concerning the angle of tilt of imaged DWNTs, has recently been applied with success to several systems of materials encapsulated within SWNTs.[15−17]

Experimental Section

The DWNTs used in this work were synthesized by the arc-evaporation procedure first described previously,[8] but with minor modifications to the experimental conditions.[18] The encapsulation of the metal halides within the DWNTs followed a general melt-phase filling procedure described elsewhere.[19] In a typical filling experiment, the chosen alkali-metal halide was mixed with the DWNTs, either in as-prepared or purified form,[18] in a drybox, and the reaction mixture was subsequently flame-sealed in a silica ampule under vacuum. Programmable Carbolite MTF tube furnaces,

* To whom correspondence should be addressed. Tel.: 00441223334474. Fax: 00441223334437. E-mail: pmfjc2@cam.ac.uk.
† Inorganic Chemistry Laboratory.
‡ Department of Materials.
§ Presently at the Department of Materials Science and Metallurgy, Pembroke Street, Cambridge, CB2 3QZ, UK.

(1) Ajayan, P. M.; Iijima, S. *Nature* **1993**, *361*, 333.
(2) Smith, B. W.; Monthioux, M.; Luzzi, D. E. *Nature* **1998**, *396*, 323.
(3) Sloan, J.; Kirkland, A. I.; Hutchinson, J. L.; Green, M. L. H. *Acc. Chem. Res.* **2002**, *35*, 1054.
(4) Tsang, S. C.; Guo, Z. J.; Chen, Y. K.; Green, M. L. H.; Hill, H. A. O.; Hambley, T. W.; Sadler, P. J. *Angew. Chem.* **1997**, *36*, 2198.
(5) Costa, P. M. F. J.; Sloan, J.; Hutchison, J. L.; Green, M. L. H. *Chem. Commun.* **2003**, 2276.
(6) Kiang, C. H.; Goddard, W. A.; Beyers, R.; Salem, J. R.; Bethune, D. S. *J. Phys. Chem.* **1994**, *98*, 6612.
(7) Kong, J.; Cassell, A. M.; Dai, H. *Chem. Phys. Lett.* **1998**, *292*, 567.
(8) Hutchison, J. L.; Kiselev, N. A.; Krinichnaya, E. P.; Krestinin, A. V.; Loutfy, R. O.; Morawsky, A. P.; Muradyan, V. E.; Obraztsova, E. D.; Sloan, J.; Terekhov, S. V.; Zakharov, D. N. *Carbon* **2001**, *39*, 761.
(9) Ren, W.; Li, F.; Chen, J.; Bai, S.; Cheng, H.-M. *Chem. Phys. Lett.* **2002**, *359*, 196.
(10) Lozovik, Y. E.; Minogin, A. V.; Popov, A. M. *Phys. Lett. A* **2003**, *313*, 112.
(11) Moravsky, A. P.; Loufty, R. O. Patent Cooperation Treaty WO 02/30816 A1, 2002.
(12) Saito, R.; Matsuo, R.; Kimura, T.; Dresselhaus, G.; Dresselhaus, M. S. *Chem. Phys. Lett.* **2001**, *348*, 187.
(13) Khlobystov, A. N.; Britz, D. A.; Ardavan, A.; Briggs, G. A. D. *Phys. Rev. Lett.* **2004**, *92*, 245507.
(14) Flahaut, E.; Sloan, J.; Coleman, K.; Williams, V. C.; Friedrichs, S.; Hanson, N.; Green, M. L. H. *Mater. Res. Soc. Symp. Proc.* **2001**, *633*, A13.15.
(15) Coene, W.; Janssen, G.; Beeck, M. O. d.; Dyck, D. V. *Phys. Rev. Lett.* **1992**, *69*, 3743.
(16) Meyer, R. R.; Sloan, J.; Dunin-Borkowski, R. E.; Kirkland, A. I.; Novotny, M. C.; Bailey, S. R.; Hutchison, J. L.; Green, M. L. H. *Science* **2000**, *289*, 1324.
(17) Meyer, R. R.; Kirkland, A. I.; Saxton, W. O. *Ultramicroscopy* **2002**, *92*, 89.
(18) Costa, P. M. F. J.; Friedrichs, S.; Sloan, J.; Green, M. L. H. *Carbon* **2004**, *42*, 2527.
(19) Brown, G.; Bailey, S. R.; Novotny, M.; Carter, R.; Flahaut, E.; Coleman, K. S.; Hutchison, J. L.; Green, M. L. H.; Sloan, J. *Appl. Phys. A* **2003**, *76*, 457.

10.1021/cm050299q CCC: $30.25
Published on Web 05/17/2005

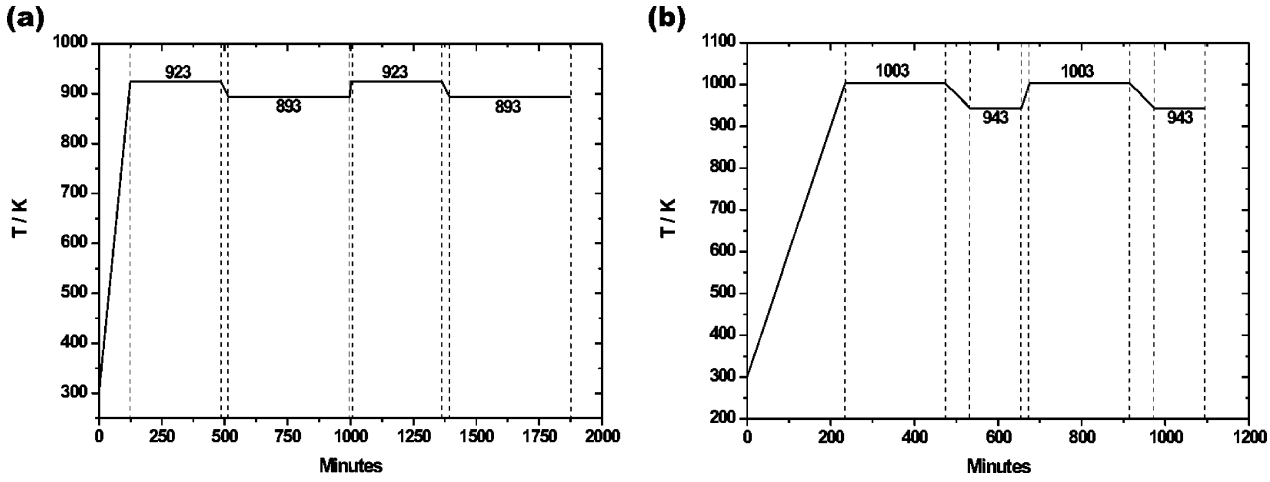

Figure 1. (a) Schematics of the heating cycle used for the KI@DWNT sample (c). (b) Heating cycle for the CsI@DWNT experiment.

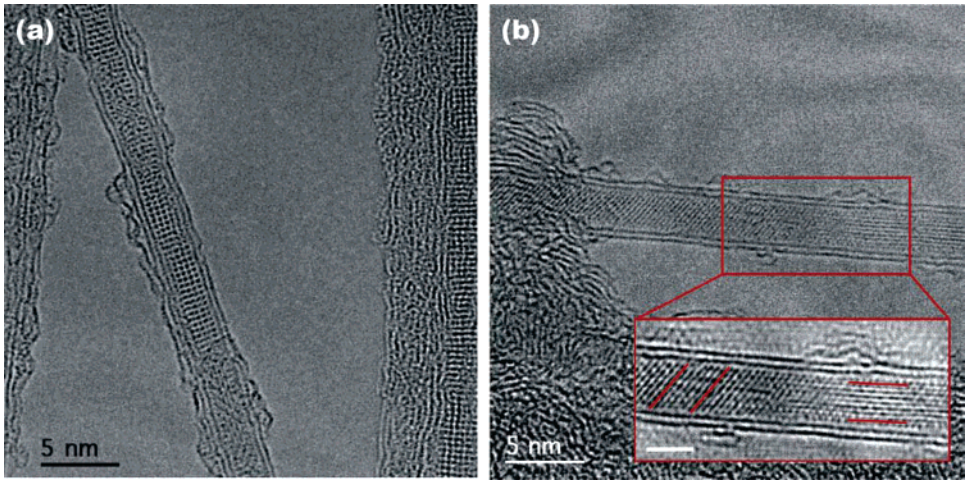

Figure 2. HRTEM images of typical isolated DWNTs filled with crystalline KI from sample (c). (a) DWNT with an external diameter (d_{ext}) of 3.04 nm and an internal diameter (d_{int}) of 2.23 nm containing a rocksalt KI crystal viewed along the ⟨100⟩ axis. (b) Filled tube with $d_{ext} = 3.47$ nm and $d_{int} = 2.66$ nm. The noise-filtered image inset shows a section of the KI crystal where rotation of the lattice planes is seen resulting in different viewing projections of the halide structure. The bar is 2 nm.

fitted with Eurotherm 2416 CC control systems, were employed to carry out the melt-phase filling of the nanotubes. Three individual samples of KI@DWNT composite were prepared, using different conditions albeit keeping an approximate 1:1 molar ratio of nanotubes:KI. For sample (a), a reaction mixture of 30 mg of as-prepared (unpurified) DWNTs and 21 mg of dried KI (Aldrich, 99%) was heated to 1003 K at a ramp rate of 10 K min^{-1}, followed by a dwell time of 240 min. The sample was allowed to cool to room temperature inside the furnace. For sample (b), 30 mg of purified DWNTs was mixed with 83 mg of dry KI and subjected to a heating cycle, identical to that for sample (a). For sample (c), a reaction mixture identical to that of sample (b) was heated using the cycle shown in Figure 1a. At the end of the heating cycle, the furnace was switched off and the sample was allowed to cool.

The CsI@DWNT composite was prepared using 30 mg of purified DWNTs and 130 mg of dry CsI (Aldrich, 99.9%) in an evacuated silica ampule. The heating cycle is represented schematically in Figure 1b.

After the cooling, the ampules were opened and the products were suspended by sonication in ethanol. The resulting dispersion was placed dropwise onto 3.0 mm copper grids coated with a lacey carbon film (Agar) to prepare the samples for HRTEM analysis. The samples were analyzed using both a JEOL JEM-4000EX operated at 400 kV and a JEOL JEM-3000F operated at 300 kV. The focal series and EDX spectra of selected filled DWNTs were acquired on the JEOL JEM-3000F, equipped with a GATAN 794 (1k × 1k pixel) CCD camera. All focal series consisted of 20 images, acquired automatically at a magnification of ×600 000, with a focal increment of ca. 15 nm between successive images and an exposure time of 0.5 s per image. The last image of each series was acquired at the same focus level as the first image, to account for possible sample drift and specimen damage during the total acquisition time. Using the focal series dataset, the final resolution of the restored images is ultimately the information limit of the JEM-3000F microscope, that is, 1 Å. For all samples, EDX spectroscopy was employed to confirm the presence of the alkali-metals and iodine.

Results

(i) KI@DWNT. In 2000, Meyer et al. described the individual positions of the potassium and iodine ions within a KI@SWNT system in which a 1.6 nm nanotube contained a 3 × 3 KI crystal. In this study, the lattice spacings of the KI crystal were shown to be significantly different from those for bulk KI.[16] A subsequent report described a 1.4 nm SWNT filled with a 2 × 2 KI crystal that exhibited expansion of the KI lattice spacing by as much as 14% as compared to the bulk KI.[20] For both studies, the filling yields were estimated to be between 30% and 50%. The DWNTs filled with KI were found to exhibit significantly lower filling

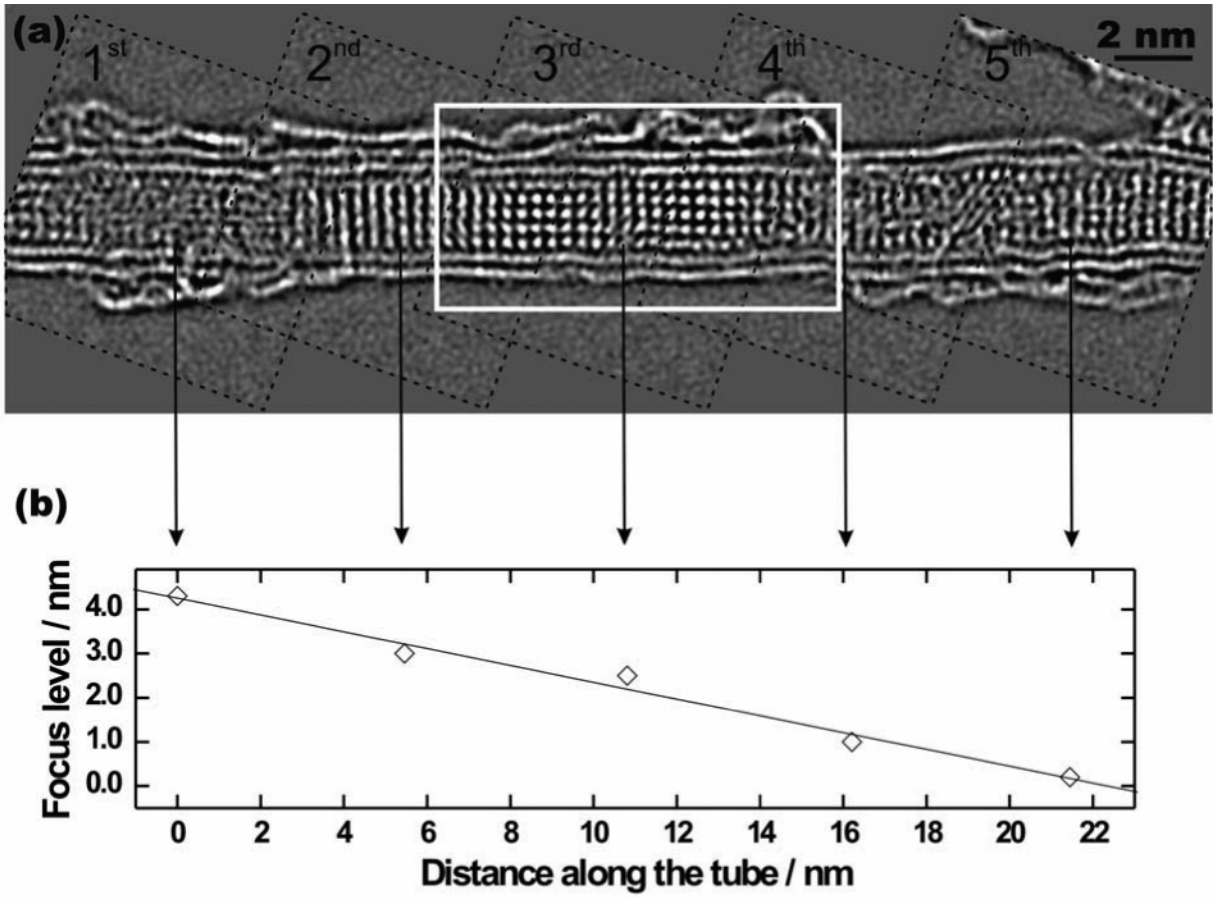

Figure 3. (a) Restored phase of the KI@DWNT encapsulation composite, also shown in Figure 2a. The centers of the five subregions are indicated with arrows, and the rectangular white box defines the composite section studied in detail (see below). (b) Diagram showing measured focus levels for the individual subregions plotted against their displacements along the tube. The best-fitting line demonstrates the gradual decrease of the focus levels from the first to the fifth subregion.

yields. Sample (a) was prepared using higher temperatures and longer dwell times than for the equivalent reported KI@SWNT composite but resulted in filling yields estimated to be ~10%. This lower filling yield can be understood if both layers of the tube ends are initially closed, making it more difficult for the melted KI to progress into the DWNTs. This filling yield was improved by a factor of 2 when purified DWNTs were used, and this is possibly a consequence of the acid and air oxidation treatments giving a higher proportion of open-ended tubes. However, the resulting filling yield of 20% was significantly lower than that reported for KI@SWNT. Sample (c) was subjected to an alternating heating cycle, resulting in a filling yield of 30%, which approaches the lower values found for corresponding SWNTs experiments.[16,20]

Figure 2 shows two HRTEM images of DWNTs, filled with crystal fragments of KI in the rocksalt form, as was observed for the majority of KI@DWNT composites imaged.

The KI@DWNT composite shown in Figure 2a was also analyzed using the image restoration approach. The restored phase shown in Figure 3a was obtained using only the first six images of the 20-membered focal series of HRTEM micrographs, because the KI crystal had rearranged after ca. 30 s exposure to the electron beam. The phase-imaged composite was separated into five overlapping subregions (300 × 300 pixels) along the major tube axis, and each of the subregions was restored independently, to account for nonlinear movements of the object during the acquisition of the focal series (Figure 3a). This modification enabled the determination of an absolute focus value for each of the subregions and the plot of these values versus the subregion displacements along the tube, which results in the inclination angle β of the overall composite with respect to the image plane of the electron microscope as described previously.[21]

The plot given in Figure 3b shows a systematic decrease in the focus from left to right (i.e., the left end, first subregion with $x = 0$, is closer to the viewer than the right end, fifth subregion), with an inclination angle of $\beta = 10.8° \pm 0.8°$. The average diameters of the inner (2.23 nm) and outer (3.04 nm) tubes corresponded approximately to an inner SWNT of (11,22) conformation ($d_t = 2.231$ nm) and an outer SWNT of (18,26) conformation ($d_t = 3.041$ nm), respectively, and the DWNT was therefore modeled and simulated as a (11,22)SWNT@(18,26)SWNT pair. It should be noted that several lattice defects were observed within both of the nested graphene cylinders, giving rise to slight diameter variations along the DWNT.[18]

(20) Sloan, J.; Novotny, M. C.; Bailey, S. R.; Brown, G.; Xu, C.; Williams, V. C.; Friedrichs, S.; Flahaut, E.; Callender, R. L.; York, A. P. E.; Coleman, K. S.; Green, M. L. H.; Borkowski, R. E.; Hutchison, J. L. *Chem. Phys. Lett.* **2000**, *329*, 61.

(21) Friedrichs, S.; Sloan, J.; Green, M. L. H.; Hutchison, J. L.; Meyer, R. R.; Kirkland, A. I. *Phys. Rev. B* **2001**, *64*, 045406.

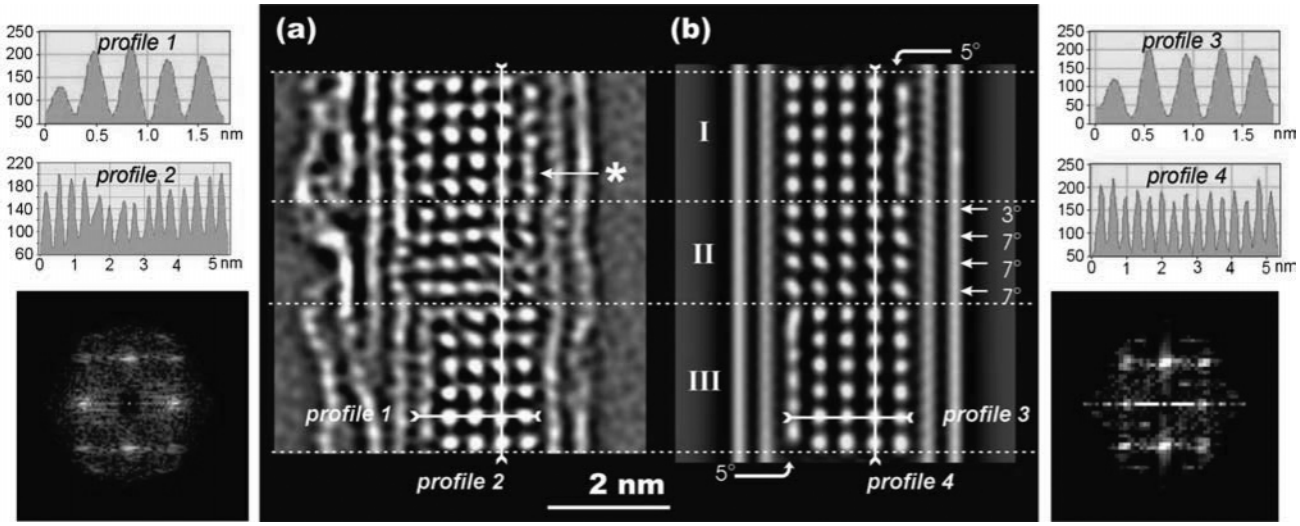

Figure 4. Composite picture illustrating the comparison of the restored and simulated phase of a KI@DWNT encapsulation composite, given in Figure 3a (also shown in Figure 2a as a single-axial HRTEM image). (a) Selected central region of the restored phase; the star signals an interstitial extra column of atoms, and the marked line profiles 1 and 2 are displayed to the left of (a), together with the fast Fourier transform (FFT) of the displayed region. (b) Simulated image of the final composite model with the same inclination angle (10°) and contrast transfer function of the restored image. The additional inclinations and plane rotations considered in the different subsections (I to III) of the model are indicated. To the right of (b) are the line profiles taken and the FFT of the simulated image.

The image reproduced in Figure 3a shows that the KI@DWNT is filled continuously within the restored region but that the filling material displays an ordered, crystalline arrangement only in the central ~9 nm region indicated by the white frame. This region of the restored phase was subsequently used for a detailed structural analysis of the encapsulated crystal fragment. Line profiles were obtained to measure the distances between the columns of superimposed atoms (bright dots) both along and across the major axis of the nanotube, as illustrated in Figure 4a.

Line profile 1 shows a strong similarity of measured phase contrast intensities across a row of peaks perpendicular to the long DWNT axis (with the exception of the first peak of the profile, which relates to a distorted row of KI, beside the tube walls), indicating that the number of atoms present in each column is constant. The average spacings between the columns were 0.37 ± 0.03 nm across the major axis of the DWNT (profile 1), and 0.36 ± 0.03 nm along the major axis (profile 2) (in both cases, the error is determined by the finite pixel size of the restored image, i.e., 0.028 nm). Because the {200} *d*-spacing of the rocksalt KI in bulk form is 0.352 nm,[22] the above values indicate that hardly any expansion of the KI lattice spacings along or across the major axis of the nanotube occurred as a consequence of encapsulation.

The KI fragment was modeled starting from a crystal fragment of bulk KI, which was subjected to the lattice distortions and phase information extracted from the restored phase. Various crystal thicknesses were explored during the modeling process, ranging between one and five atomic layers, and the simulated phases were compared to the experimental phase to match the observed contrast variations. The best simulated phase match was found for a model containing five columns of atoms across, 15 columns in length, and only three atomic layers in projection (i.e., a 5 $\times$ 15 $\times$ 3 KI crystal fragment). This model is depicted as an unencapsulated crystal fragment in Figures 5a−d.

This optimized crystal model was subsequently placed inside the (11,22)@(18,26) DWNT and the entire composite was tilted by 10°, to match the measured inclination angle β.

Figures 5g and h shows empty space between the cylindrically drawn nanotubes and the rectangular KI fragment. It is likely that the walls of the DWNT will distort from a perfect cylindrical shape and will structurally adapt toward the crystal morphology, as was reported recently for the CoI_2 crystal formed in SWNTs.[23] The information contained in the restored phase was not sufficient to determine the overall shape of any DWNT distortion in this instance. The modeling and simulation were conducted using a model of an undistorted (11,22)@(18,26) DWNT filled with a 5 $\times$ 15 $\times$ 3 KI crystal fragment, as illustrated in Figures 5e−h.

The modeled KI fragment was divided into three subsections (i.e., **I**, **II**, and **III**), as indicated in Figure 4b, and each subsection was individually modified to model more accurately the lattice distortions observed. In subsection **I**, a plane-shearing effect was modeled: the right-most row was slightly displaced (~0.12 nm) in the direction of the major axis of the tube, so that the columns of atoms in this row would be out-of-line with respect to the rest of the rows across the tube axis. Additionally, an extra inclination for this row of 5° (added to the 10° tilt described above) was modeled. An equivalent distortion was also applied to the left-most row of subsection **III** (i.e., displacement of the atom columns and additional inclination of 5°). For subsection **II**, the four rows across were rotated orthogonally by 3° or 7°, resulting in an atom staggering effect that attempts to reproduce the contrast smearing observed in the phase image.

The resulting KI@DWNT model, shown in Figures 5e and g (i.e., projected along the ⟨100⟩ direction of the KI

(22) Cortona, P. *Phys. Rev. B* **1992**, *46*, 2008.

(23) Philp, E.; Sloan, J.; Kirkland, A. I.; Meyer, R. R.; Friedrichs, S.; Hutchison, J. L.; Green, M. L. H. *Nat. Mater.* **2003**, *2*, 788.

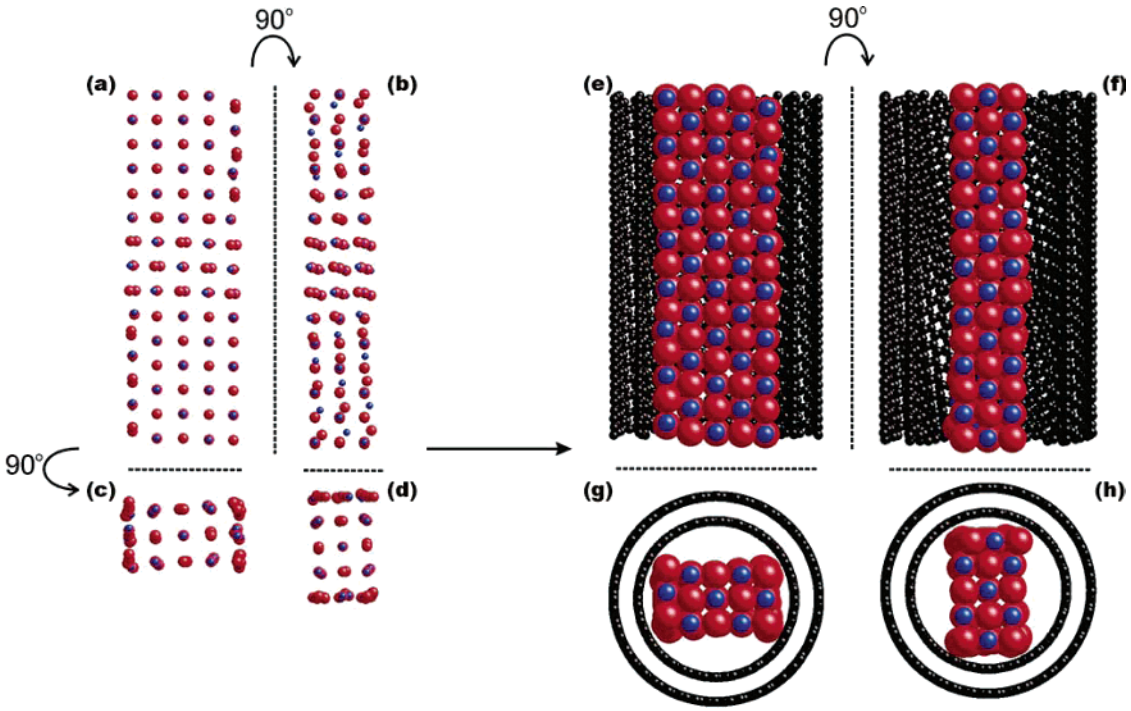

Figure 5. Model representations for the KI fragment and the KI@DWNT section analyzed. For clarity, the inclination angle of the tube ($\beta = 10°$) has been omitted. (a) KI fragment viewed along the ⟨100⟩ direction. (b) Crystal in (a) rotated by 90° along the DWNT's major axis (i.e., viewed along the ⟨001⟩ direction of the bulk KI crystal). Parts c and d show end-on-views of (a) and (b), respectively. (e) "Space-filling" model of the whole composite viewed along the KI ⟨100⟩ direction (part of the tube was suppressed for clarity). (f) The model in (e) was rotated 90° along the tube's major axis. Parts (g) and (h) are end-on-views of (e) and (f), respectively.

fragment), was subjected to a standard multislice simulation procedure using the contrast transfer function (CTF) of the experimental restored phase to account for the microscope information limit in the restoration process and any residual aberrations.[21] The obtained simulated phase provides an excellent match with the experimental phase (compare Figures 4a and b). Line profiles, taken across (profile 3) and along (profile 4) the simulated crystal, are also commensurate with those obtained from the experimental phase, concerning both lattice spacings and relative contrast variations (cf., profiles 1 and 2, respectively). Although the modeled KI lattice defects can reproduce part of the observed distortions, it should nevertheless be pointed out that other disorder factors are observed in the restored image, that are not included in the model. For instance, extra atoms (or columns of atoms), present in interstitial sites, are observed along the distorted rows in the different subsections (one of these is marked in Figure 4a with a star).

(ii) CsI@DWNT. In its bulk form, CsI crystallizes commonly in either the rocksalt or the CsCl-type structural forms. In CsI@SWNT, where filling yields attained 40%, it was reported that the rocksalt form was predominant.[19]

CsI@DWNT samples were prepared using purified DWNTs and the melt-phase filling procedure, resulting in filling yields of ∼25%. The images shown in Figure 6 illustrate various examples of typical CsI@DWNT composites in which the CsI crystal fragments adopt predominantly the rocksalt structural form. One example of a DWNT apparently filled with a CsCl-type structure is also shown (Figure 6c). The area indicated in Figure 6c possibly shows CsI either in the rocksalt structure viewed in the projection along the ⟨111⟩ axis or the CsCl structure as viewed along the ⟨111⟩ axis. However, models and HRTEM image simulations produced using the standard multislice algorithm showed that the distances between the columns of atoms of ∼3.9 Å, both along the tube major axis and diagonally, and the uniformity of contrast of the crystal lattice across the tube, are only consistent with the CsCl-type (Figure 6d).

Figure 7 shows another example of a CsI@DWNT composite analyzed using the image restoration approach. The phase displayed in Figure 7a was restored using only three images of the 20-membered focal series, separated into seven individual, overlapping subregions of 300 × 300 pixels. This composite is similar to the KI@DWNT composite described above in that the ordering of the encapsulated halide crystal is not constant throughout the filling material and exhibits severely distorted fragments. Figure 7b shows the focus level of each individually restored subregion plotted versus the distance along the nanotube and illustrates the inclination angle (calculated as $\beta = 7.2° \pm 0.8°$), with the left end (first subregion) of the composite lying lower in the electron beam (i.e., farther to the viewer) than the right end (seventh subregion). The diameters of both nesting graphene cylinders were determined (inner cylinder, 2.51 nm; outer cylinder, 3.19 nm), and the best matching SWNTs ((8,27), $d_t = 2.52$ nm for the inner tube and (16,30), $d_t = 3.21$ nm for the outer tube) were subsequently used to model and simulate the observed DWNT.

A detailed structural analysis of the encapsulated CsI fragment was conducted on one of the well-ordered sections, indicated by the white frame in Figure 7a. The restored phase was sampled with line profiles, running parallel and perpendicular to the DWNT's major axis. This determined the average distance between projected columns of atoms as 0.38

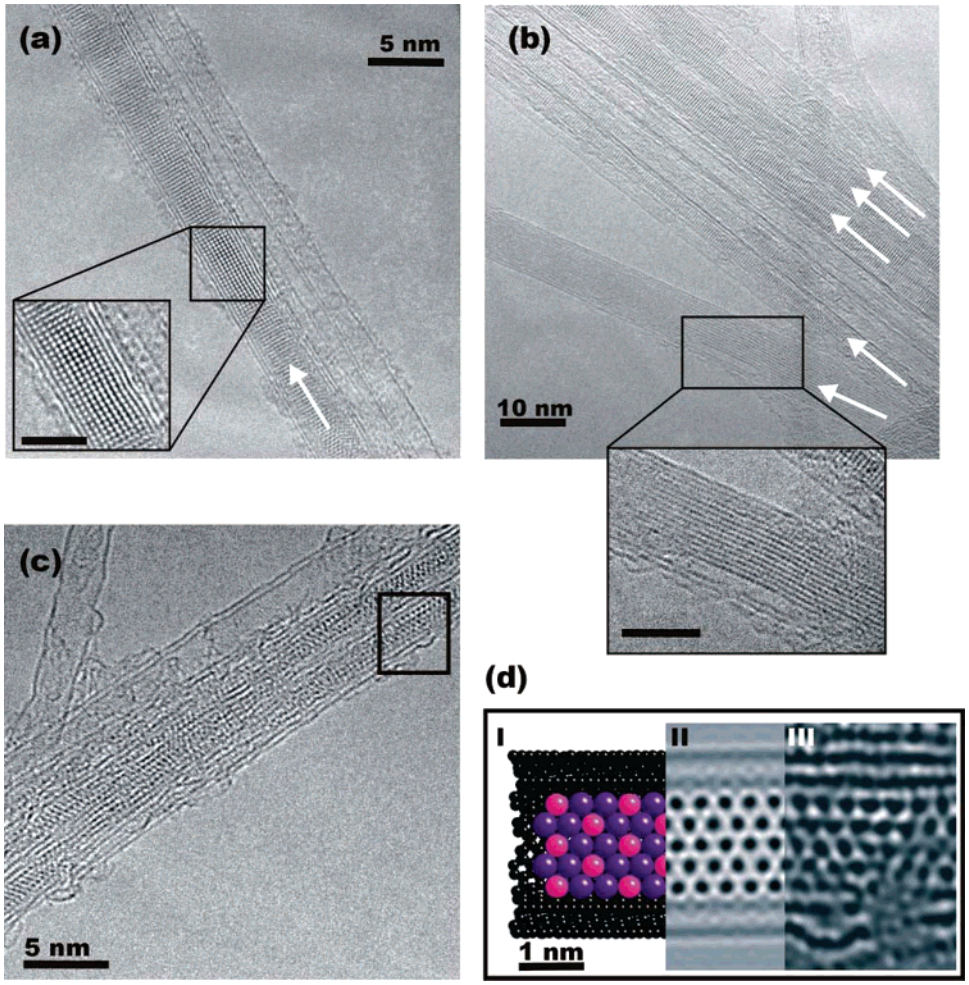

Figure 6. (a) Bundle of DWNTs containing a DWNT filled with crystalline CsI (diameter of the inner tube, 3.9 nm; diameter of the outer tube, 4.7 nm). The inset image shows the rocksalt structure of the encapsulated CsI. Scale bar is 2 nm. (b) A bundle of DWNTs partially filled with CsI with the filled tubes indicated by white arrows. The outset image shows the CsI lattice plane fringes along the tube axis, as well as a defect in the crystal structure in which some lattice planes nearer to the tube inner wall appear to be incomplete whereas others seem to bend. The inner tube is 5.7 nm in diameter, and the outer is 6.5 nm. The scale bar of the outset image is 5 nm. (c) A bundle of DWNTs, three of which are filled with crystalline CsI (a large SWNT is also shown in the upper left-hand corner). The encapsulated crystal fragment of the bundle-edge DWNT exhibits a CsCl-type structure. (d) Study of the composite marked in (c): I, model of a section of CsI@DWNT; II, simulated HRTEM image of the model in I; III, high-frequency noise-filtered HRTEM image of part of the section marked in (c).

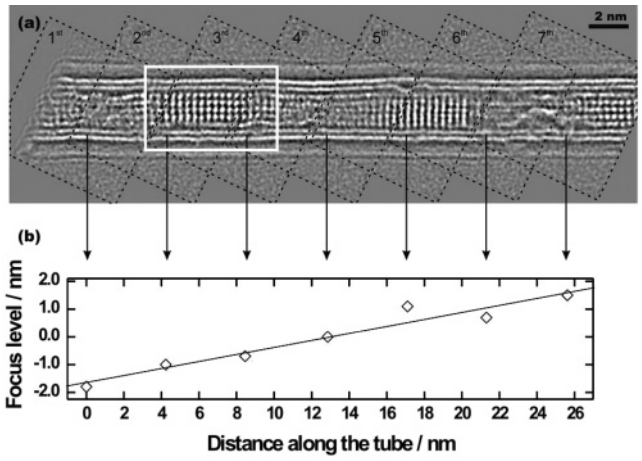

Figure 7. (a) Restored DWNT filled with CsI showing three individual sections of crystalline CsI fragment separated by zones in which no crystal contrast can be observed. The white box indicates the section chosen for detailed structural analysis (see below). (b) Plot of the focus levels versus displacement of the subregions along the tube indicating an increase of the focus from left to right which results in an inclination angle of 7°.

$\pm$ 0.03 nm (cf., profile 1) and 0.38 $\pm$ 0.03 nm (cf., profile 2) along these directions, respectively, as illustrated in Figure 8a. These values are commensurate with the reported {002} *d*-spacing for the rocksalt form of bulk CsI (0.382 nm),[24] indicating that no observable distortion of the CsI lattice occurred during the encapsulation process.

Similar to the approach taken for the KI@DWNT composite, the encapsulated CsI fragment selected for detailed structural analysis was divided into three subsections (cf., Figure 8b). Given that the intensities of the columns in the line profiles were similar (except for the right-most row, see profile 1), the model found to provide the best-fit with the restored phase was a 5 $\times$ 12 $\times$ 4 CsI fragment, as illustrated in Figures 9a−d. This fragment was then placed in a modeled (8,27)@(16,30) DWNT, and the whole composite was tilted by 7° and rotated anticlockwise along the tube's major axis by 4°.

The modeled CsI fragment was subsequently subjected to the following additional distortions: for subsection **I**, one column of atoms was deleted from the right-most row with the spacing between the remaining two columns expanded

(24) Blackman, M.; Khan, I. H. *Proc. Phys. Soc., London* **1961**, *77*, 471.

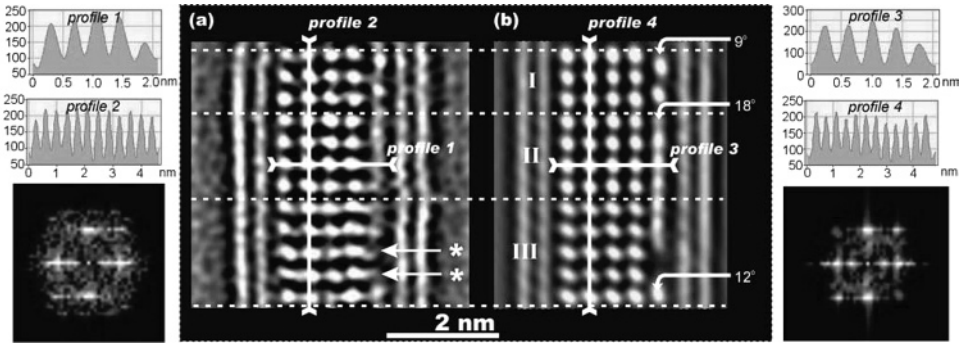

Figure 8. Comparison of the restored and simulated phases of the investigated CsI@DWNT system. (a) Selected section of the restored CsI@DWNT image chosen for analysis; the stars mark vacancy defects in the lattice structure of the CsI fragment. The line profiles, given to the left of part a, were obtained from crystal rows perpendicular and parallel to the DWNT's major axis, indicated by the white lines in (a). The bottom left corner displays a fast Fourier transform (FFT) of the selected region given in (a). (b) Simulated phase of the final composite model displayed under the same inclination angle (7°) and contrast transfer function of the restored phase. Additional inclinations were applied to the right-most row, illustrated by the white arrows and inclination magnitude. The line profiles and FFT obtained from the simulated phase are given to its right.

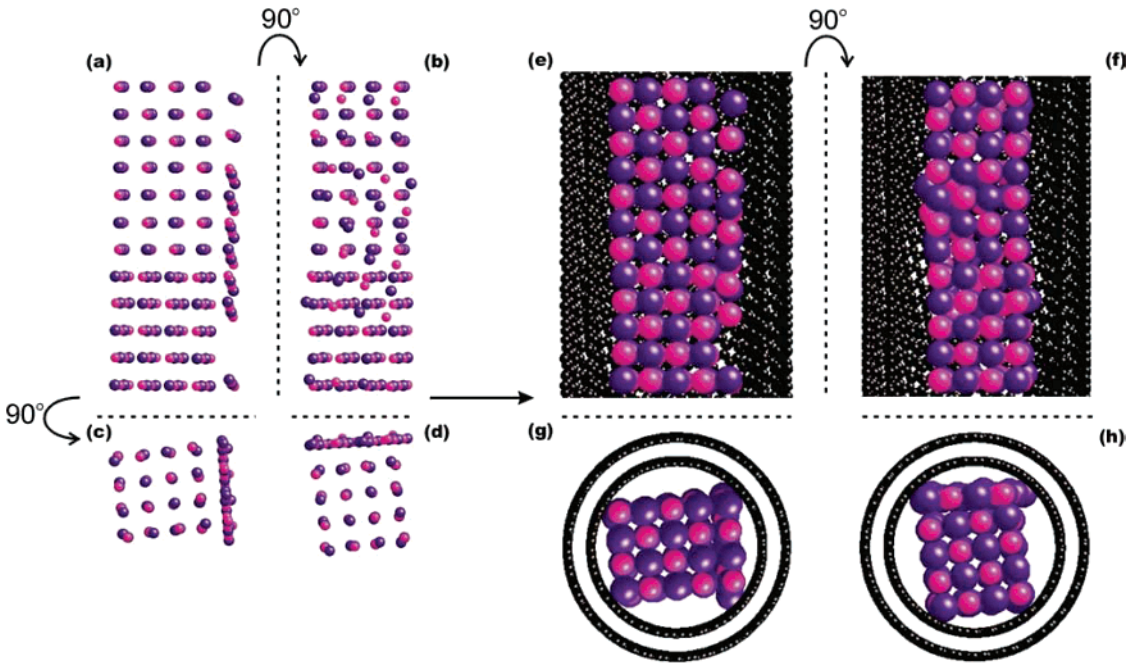

Figure 9. Model representations of the CsI crystal fragment and the CsI@DWNT encapsulation composite. For clarity, the inclination angle ($\beta = 7°$) was not applied to the models shown. (a) CsI fragment viewed along the ⟨100⟩ direction. The various distortions applied to the lattice are visible, particularly for the right-most row of the fragment. (b) Rotated crystal observed along the ⟨001⟩ direction. Parts (c) and (d) display end-on-views of (a) and (b), respectively. (e) "Space-filling" model of the whole CsI@(8,27)SWNT@(16,30)SWNT composite, viewed along the CsI ⟨100⟩ direction, with the upper half of the DWNT omitted for clarity. (f) Composite viewed along the CsI ⟨001⟩ direction. Parts (g) and (h) display end-on-views of (e) and (f), respectively.

by 20%; these were then arranged to be out-of-line with the neighboring columns, before being finally inclined by 2° (in addition to the 7° inclination of the whole composite). In subsection **II**, the right-most row was displaced along the major axis of the DWNT and further inclined by 11° (giving a total of 18° tilt). The same distortion was applied to the top two right-most atom columns of subsection **III**. For the remaining content of subsection **III**, two columns were omitted to account for the lattice vacancies seen in the restored phase (marked with stars in Figure 8a). The column of atoms in the bottom of subsection **III** was slightly displaced and tilted by an additional 5° (i.e., total inclination angle 12°). Furthermore, the whole lattice in subsection **III** was rotated anticlockwise by an additional 6°, to partially account for the observed contrast smearing.

Discussion

A comparison between our detailed structural analysis for both the KI@DWNT and the CsI@DWNT composites and the reported bulk lattice parameters of both alkali-metal halides indicates that no significant lattice distortions occur for either KI or CsI crystal fragments when encapsulated within DWNTs. This result contrasts with the much larger distortions found in KI@SWNT encapsulation composites, for which lattice expansions as high as 14% were reported.[20] However, such a discrepancy is perhaps to be expected because the larger dimensions of the crystallites encapsulated within DWNTs, particularly with respect to their widths, result in a much lower share of surface atoms, therefore maintaining, in each case, fragments which are closer to the bulk. By contrast, in the SWNT encapsulation composite,

the tube effect is much more noticeable due to the smaller nanotube dimensions and the fact that the crystals so-formed have an exceptional proportion of surface atoms.[20] The encapsulated fragments in the DWNTs are therefore more "bulk"-like than their counterparts formed within the narrower SWNTs.

Previous studies on alkali-metal iodides composites with SWNTs show that they are all stoichiometric with 1:1 cation: anion ratios.[25] This is also true for both rocksalt and CsCl-type crystallites in DWNTs. The strong tendency for the alkali-metal halides to adopt the rocksalt structure on their crystallization within nanotubes may derive not only from stoichiometric arguments but also from energetic constraints (i.e., lattice energy, crystal-to-wall contact forces). In fact, the adoption of the 6:6 rocksalt structure, with the atoms coordinated in an octahedral fashion, is expected to provide a more efficient use of the iodine 5p orbitals due to bond directionality effects.

For both encapsulated halides analyzed in this work, significant lattice defects and distortions of the DWNT encapsulated rocksalt fragments were observed. Among the possible different defects that can occur in bulk alkali halides crystallizing in the rocksalt structure, interstitials and vacancies are the most common.[26] Both types of defects were apparently observed in this work with the stars in Figures 4a and 8a marking lattice atom(s) in interstitial sites and lattice vacancies, respectively. With regard to the vacancies in Figure 8a, the proposed model assumes a cluster of vacant pairs, which results in the absence of two whole columns of atoms in the CsI crystal fragment. The interstitial occupied sites, such as the one indicated in Figure 4a, were not included in the proposed KI model. These may possibly correspond to Frenkel-type defects, but the related paired vacant sites could not be identified.

We have also observed considerable distortions of whole atomic planes amounting to layer shearing,[27] which seem to occur preferentially with layers adjacent to the carbon wall. Related plane shearing effects were also noted for AgI crystals encapsulated within SWNTs, but these were associated with strain-induced bending observed in the encapsulating nanotube.[25]

The observed occurrence of the plane rotations for the MI@DWNTs in the present work is more noticeable than that reported for the equivalent SWNTs systems. Several phenomena could explain this such as distortions at the crystal-wall interface, which may occur due to local curvature of the encapsulating DWNT. In a different approach, theoretical calculations by Wilson[28] indicate that the ionic melt exterior to the nanotube has a significant influence as a directing agent on the final encapsulated crystallite structure of KI@SWNT composites. However, due to the second graphene sheet, DWNTs could shield this exterior melt directing effect, leading to more pronounced twists parallel to the tube axis on the KI structure.

Conclusions

In the present work, we have demonstrated the first filling of DWNTs with the alkali-metal halides, KI and CsI. For both composite systems, the encapsulated materials showed no significant distortions of their respective lattice spacings relative to their bulk structure. Additionally, a preponderance of the rocksalt over the CsCl form was observed. Structural defects in the encapsulated halide materials, such as plane faults, small twists, and vacancy/interstitial defects, were described. The identification and understanding of these defects is crucial as their presence in a crystalline lattice, even in minute concentrations, may significantly affect the electronic and optical properties of the encapsulated crystals.

Further studies are needed to clarify if these lattice imperfections are induced by the characterization technique used, that is, if they are beam induced, or if they are mainly the result of natural thermodynamic restrictions imposed by the synthesis methodology employed in the production of these nanostructured composites.

Acknowledgment. We thank John Spence for comments on the manuscript during its preparation. P.M.F.J.C. is grateful to the Fundacao para a Ciencia e a Tecnologia for a graduate scholarship (SFRH/BD/3103/2000). S.F. acknowledges the HEFCE fund and the CMI for financial support. J.S. is indebt to the Royal Society for a University Fellowship.

CM050299Q

(25) Sloan, J.; Kirkland, A. I.; Hutchison, J. L.; Green, M. L. H. *C. R. Phys.* **2003**, *4*, 1063.
(26) West, A. R. *Basic Solid State Chemistry*, 2nd ed.; John Wiley & Sons: Chichester, 2000.
(27) Allpress, J. G.; Sanders, J. V.; Wadsley, A. D. *Acta Crystallogr., Sect. B* **1969**, *25*, 1156.
(28) Wilson, M. *J. Chem. Phys.* **2002**, *116*, 3027.